arXiv:cond-mat/9705168v1 15 May 1997

Stability of Uniform Shear Flow

José M. Montanero

Departamento de Electrónica e Ingeniería Electromecánica, Universidad de Extremadura,

E-06071 Badajoz, Spain

Andrés Santos

Departamento de Física, Universidad de Extremadura,

E-06071 Badajoz, Spain

Mirim Lee

TCSUH, Department of Physics, University of Houston,

Houston, TX 77204

James W. Dufty

Department of Physics, University of Florida

Gainesville, FL 32611

J. F. Lutsko

ESADG, Department of Chemical Engineering, Katholiek University of Leuvan,

B-3001, Heverlee, Belgium

(February 1, 2008)

Abstract

The stability of idealized shear flow at long wavelengths is studied in detail. A hydrodynamic analysis at the level of the Navier-Stokes equation for small shear rates is given to identify the origin and universality of an instability at any finite shear rate for sufficiently long wavelength perturbations. The

analysis is extended to larger shear rates using a low density model kinetic equation. Direct Monte Carlo simulation of this equation is compared with a hydrodynamic description including non Newtonian rheological effects. The hydrodynamic description of the instability is in good agreement with the direct Monte Carlo simulation for $t < 50t_0$, where t_0 is the mean free time. Longer time simulations up to $2000t_0$ are used to identify the asymptotic state as a spatially non-uniform quasi-stationary state. Finally, preliminary results from molecular dynamics simulation showing the instability are presented and discussed.

PACS numbers: 47.20.Ft, 47.15.Fe, 05.20.Dd, 05.60.+w

Typeset using REVTEX

I. INTRODUCTION

Uniform shear flow is a prototype non-equilibrium state admitting detailed study at both the macroscopic and microscopic levels via theory and computer simulation. This is an idealized version of shear flow between parallel plates in which the velocity profile is exactly linear in a coordinate orthogonal to the flow direction (as in Couette flow) and with a spatially uniform temperature and pressure (in contrast to Couette flow). There is a single scalar control parameter, the shear rate a, which measures how far the system is driven from equilibrium. This flow is generated by periodic boundary conditions in the local Lagrangian frame (Lees-Edwards boundary conditions) that can be implemented at the levels of hydrodynamics, kinetic theory, and Newtonian mechanics [1–3]. Although these boundary conditions are non-local and therefore not reproducible in real experiments, they are ideally suited for computer simulation of this special nonequilibrium state and for more penetrating theoretical analysis. In this way, a quantitative study of rheological properties usually associated with complex molecular systems has been performed for simple atomic fluids [4]. The most complete studies have been via molecular dynamics simulation of Newtonian dynamics at high densities and, more recently, by Monte Carlo simulation of the Boltzmann equation at low densities [5,6]. Molecular dynamics simulations have revealed a transition from fluid symmetry to an ordered state at sufficiently high shear rates [7], which has been attributed to a short wavelength hydrodynamic instability [8]. The objective here is to show that uniform shear flow also is unstable at sufficiently long wavelengths, for any finite value of the shear rate [9,10]. This instability has not been seen in earlier computer simulations due to the small system sizes considered, with consequent restrictions to shorter wavelengths. The instability is identified theoretically from a hydrodynamic analysis both near and far from equilibrium. This analysis is confirmed quantitatively at short times by Monte Carlo simulations of an associated low density kinetic equation. The asymptotic evolution of this instability also is explored via Monte Carlo simulation showing transition to a non-steady, spatially inhomogeneous state superimposed upon the uniform shear flow.

Finally, the instability is demonstrated by new molecular dynamics simulations on larger systems to allow consideration of long wavelengths. This instability does not invalidate or compromise in any way previous studies of uniform shear flow, since we also establish that the flow is stable at sufficiently short wavelengths.

The boundary conditions generate viscous heating so that uniform shear flow is not stationary. This viscous heating can be controlled by the introduction of a non-conservative external force that acts as a uniform thermostat. The simplest choice is a Stokes law drag force on each particle proportional to its velocity relative to the local macroscopic flow. The proportionality "constant" then is adjusted to compensate for the heating. There are several possibilities in the detailed implementation of the thermostat, leading to the same properties for the stationary state but different hydrodynamics for small perturbations from that state. The theory and Monte Carlo simulations are carried out for both global and local thermostats. The role of the thermostat is studied in the Appendix where it is shown that the qualitative features of the instability are not sensitive to the choice of thermostat.

In the next section, the usual Navier-Stokes hydrodynamic equations are considered. These equations are restricted to small gradients of the hydrodynamic fields relative to equilibrium, and consequently the shear rate must be small in this analysis. Otherwise, the density and interatomic force law can be considered arbitrary within the fluid phase. The stationary solution for uniform shear flow is identified, and the linear hydrodynamic equations for small perturbations of this solution are studied. The five hydrodynamic modes are determined in detail for the special case of spatial perturbations orthogonal to the flow. A critical wavevector, $k_c(a)$, is determined such that for wavevectors $k < k_c(a)$ the perturbations grow as a function of time. The critical wavevector vanishes as the shear rate a goes to zero, but for any finite value of the shear rate there are sufficiently small wavevectors (long wavelengths) such that the perturbation is unstable.

These hydrodynamic predictions are tested by comparison to Monte Carlo simulations at the more fundamental kinetic theory level. A model kinetic equation has been analyzed for states near uniform shear flow, without restriction on the shear rate [10]. The hydrodynamic

equations for small deviations from uniform shear flow determine the critical wavevector, $k_c(a)$, for values of the shear rate a beyond the limitations of the Navier-Stokes equations where efficient Monte Carlo simulations are possible. The theoretical prediction of the growth of initial perturbations is compared with a direct Monte Carlo simulation of a solution to the kinetic equation. The results confirm both the hydrodynamic analysis and the prediction of an instability for times up to about $50t_0$, where t_0 is the mean free time, after which the initial growth has exceeded the limitations of the linear stability analysis. The simulation results are continued up to $2000t_0$ to explore the ultimate stabilization by non-linear effects. The asymptotic state for the hydrodynamic fields appears to be a system size dependent standing wave with a period of about $50t_0$. Further details and discussion are given in section III.

In section IV some preliminary attempts to see the instability at high densities using molecular dynamics for the hard sphere fluid are discussed. The system dimension in the direction of the spatial perturbation is increased by an order of magnitude relative to previous simulations. A long wavelength perturbation is found to grow on a very long simulation time, with no indication of approach to the steady uniform shear flow. A quantitative comparison with theory at the required larger densities and shear rates is now possible using a recently developed kinetic model for the hard sphere Enskog equation for application [11], although the details have not been worked out at this point. The results of the theory and simulations are summarized and discussed in section V.

II. NAVIER-STOKES ANALYSIS

On sufficiently large space and time scales the dynamics of a fluid is well-described by hydrodynamic equations obtained from the exact conservation laws for the average mass, energy, and momentum densities, together with approximate constitutive equations for the associated fluxes. For the analysis here we use the density, $n(\mathbf{r},t)$, temperature, $T(\mathbf{r},t)$, and flow velocity, $\mathbf{U}(\mathbf{r},t)$, as dependent variables rather than the density, energy density, and

momentum. The general form of these conservation laws is [12]

$$D_t n + n\nabla \cdot \mathbf{U} = 0, \tag{2.1}$$

$$D_t T + (\gamma - 1)\alpha^{-1}\nabla \cdot \mathbf{U} + (mnC_v)^{-1}\left(\nabla \cdot \mathbf{q} + P_{ij}\partial_j U_i - w\right) = 0, \tag{2.2}$$

$$D_t U_i + \rho^{-1}\partial_i p + \rho^{-1}\partial_j P_{ij} = 0, \tag{2.3}$$

where $D_t \equiv \partial_t + \mathbf{U}\cdot\nabla$ is the material derivative. The parameters occurring in these equations are the mass density, $\rho = mn$, the specific heat at constant volume, C_v, the pressure, p, the ratio of specific heats at constant pressure and volume, $\gamma = C_p/C_v$, and the coefficient of expansion, $\alpha = -n^{-1}\left(\partial n/\partial T\right)_p$. These parameters are the same functions of the local density and temperature as in equilibrium. Finally, the irreversible heat and momentum fluxes are denoted by $\mathbf{q}$ and P_{ij}, respectively, and $w = w(n, T)$ is the rate at which work is done by the external force representing the thermostat. Its detailed form will not be required in this section.

The above equations are incomplete until constitutive equations for the fluxes are specified in terms of the hydrodynamic fields. However, the special solution of uniform shear flow exists independent of this choice. It is defined by a spatially constant temperature, density, heat flux and momentum flux, and a flow velocity whose only non-vanishing component is $U_{s,x} = ay$. The shear rate, a, provides the single control parameter measuring the deviation from equilibrium. The boundary conditions are simple periodic conditions in the local Lagrangian coordinate frame, $\mathbf{r}' = \mathbf{r} - \mathbf{U}_s(\mathbf{r})t$. Substitution of these assumptions for $n = n_s$, $T = T_s$, and $\mathbf{U} = \mathbf{U}_s$ into the above conservation laws shows that (2.1) and (2.3) are satisfied, while (2.2) reduces to

$$\partial_t T_s = -(mn_s C_{v,s})^{-1}\left(aP_{s,xy} - w(n_s, T_s)\right). \tag{2.4}$$

This expresses the temperature evolution as a competition between the viscous heating effect, $\propto aP_{s,xy}$, and the cooling by the thermostat, $\propto w(n_s, T_s)$. A steady state is obtained by choosing the thermostat to cancel the viscous heating,

$$aP_{s,xy} = w(n_s, T_s). \tag{2.5}$$

The various thermostats described in the Appendix all satisfy (2.5) but differ for states away from the steady state.

Next consider the equations for small deviations of the hydrodynamic variables from the uniform shear flow state, retaining only terms linear in these deviations. To proceed it is necessary to specify the constitutive equations for the heat and momentum fluxes. In this section, attention is limited to small spatial gradients, including the shear rate, so that Fourier's law and Newton's viscosity law apply,

$$\mathbf{q} = -\kappa \nabla T, \tag{2.6}$$

$$P_{ij} = -\eta(\partial_i U_j + \partial_j U_i - \frac{2}{3}\delta_{ij}\nabla \cdot \mathbf{U}) - \eta' \delta_{ij} \nabla \cdot \mathbf{U}. \tag{2.7}$$

Here $\kappa(n,T)$ is the thermal conductivity, $\eta(n,T)$ is the shear viscosity, and $\eta'(n,T)$ is the bulk viscosity. It follows immediately that

$$\mathbf{q}_s = 0, \qquad P_{s,ij} = -\eta_s a \left(\delta_{ix}\delta_{jy} + \delta_{iy}\delta_{jx}\right), \tag{2.8}$$

$$\delta\mathbf{q} = -\kappa_s \nabla \delta T, \tag{2.9}$$

$$\delta P_{ij} = -\eta_s(\partial_i \delta U_j + \partial_j \delta U_i - \frac{2}{3}\delta_{ij}\nabla \cdot \delta\mathbf{U}) - \eta_s' \delta_{ij} \nabla \cdot \delta\mathbf{U} - a\left(\delta_{ix}\delta_{jy} + \delta_{iy}\delta_{jx}\right)\left(\eta_{s,n}\delta n + \eta_{s,T}\delta T\right). \tag{2.10}$$

An abbreviated notation has been introduced where the subscript s on a quantity indicates it is evaluated at n_s, T_s. Also, $p_{s,n} \equiv \partial p(n_s,T_s)/\partial n_s$, $p_{s,T} \equiv \partial p(n_s,T_s)/\partial T_s$, $\eta_{s,n} \equiv \partial \eta(n_s,T_s)/\partial n_s$, $\eta_{s,T} \equiv \partial \eta(n_s,T_s)/\partial T_s$, etc. With these results, the closed set of linear hydrodynamic equations for perturbations of uniform shear flow at small shear rates are given by

$$\left(\partial_t + \mathbf{U}_s \cdot \nabla\right)\delta n + n_s \nabla \cdot \delta\mathbf{U} = 0, \tag{2.11}$$

$$(\partial_t + \mathbf{U}_s \cdot \nabla)\,\delta T + (\gamma_s - 1)\alpha_s^{-1}\nabla \cdot \delta\mathbf{U} + (mn_s C_{v,s})^{-1}\left(-\kappa_s \nabla^2 \delta T - 2\eta_s a\,(\partial_x \delta U_y + \partial_y \delta U_x)\right)$$
$$= (mn_s C_{v,s})^{-1}\left(a^2\,(\eta_{s,n}\delta n + \eta_{s,T}\delta T) + \delta w\right), \quad (2.12)$$

$$(\partial_t + \mathbf{U}_s \cdot \nabla)\,\delta U_i + \delta_{ix} a \delta U_y + \rho_s^{-1}\,(p_{s,n}\partial_i \delta n + p_{s,T}\partial_i \delta T) + \rho_s^{-1}\partial_j \delta P_{ij} = 0. \quad (2.13)$$

In this section we choose a local thermostat for which δw in the temperature equation compensates for the excess viscous heating due to perturbations of the temperature and density,

$$\delta w = -a^2\,(\eta_{s,n}\delta n + \eta_{s,T}\delta T)\,. \quad (2.14)$$

This does not imply a constant local temperature, however, except for spatially homogeneous deviations from uniform shear flow, although it does lead to a constant average temperature or kinetic energy for the whole system.

These differential equations have constant coefficients which suggests an equivalent algebraic form using Fourier and Laplace transformation. Consider first the Fourier transform. The boundary conditions are periodic in the local Lagrangian frame given by $r_i' \equiv r_i - U_{s,i}(\mathbf{r})t = \Lambda_{ij}(t)r_j$, where $\Lambda_{ij}(t) \equiv \delta_{ij} - a\delta_{ix}\delta_{jy}t$, so it is appropriate to define the transform with respect to the variable $\mathbf{r}'$,

$$\delta\widetilde{y}_\alpha(\mathbf{k},t) = \int d\mathbf{r}' e^{i\mathbf{k}\cdot\mathbf{r}'}\delta y_\alpha(\mathbf{r},t) = \int d\mathbf{r} e^{i\mathbf{k}(t)\cdot\mathbf{r}}\delta y_\alpha(\mathbf{r},t), \quad (2.15)$$

where $\delta y_\alpha(\mathbf{r},t)$ denotes the set of perturbations, considered as a function $\mathbf{r}'$ in the first equality. The periodic boundary conditions require $k_i = 2n_i\pi/L_i$, where n_i are integers and L_i are the linear dimensions of the system. However, since the time derivative in the hydrodynamic equations is taken at constant $\mathbf{r}$, the representation following the second equality is useful with $k_i(t) \equiv k_j\Lambda_{ji}(t)$. The Fourier transformed hydrodynamic equations are

$$\partial_t \delta\widetilde{y}_\alpha + \left(A(a) - ik(t)B(a) + k^2(t)D\right)_{\alpha\beta}\delta\widetilde{y}_\beta = 0. \quad (2.16)$$

The three matrices $A(a)$, $B(a)$, and D are

$$A_{\alpha\beta} = a\delta_{\alpha 3}\delta_{\beta 4}, \tag{2.17}$$

$$B_{\alpha\beta}(a) = \begin{pmatrix} 0 & 0 & n_s\widehat{k}_x & n_s\widehat{k}_y & n_s\widehat{k}_z \\ 0 & 0 & c_1\widehat{k}_x - 2a\eta_s c_2\widehat{k}_y & c_1\widehat{k}_y - 2a\eta_s c_2\widehat{k}_x & c_1\widehat{k}_z \\ \rho_s^{-1}\left(\widehat{k}_x p_{s,n} - \widehat{k}_y a\eta_{s,n}\right) & \rho_s^{-1}\left(\widehat{k}_x p_{s,T} - \widehat{k}_y a\eta_{s,T}\right) & 0 & 0 & 0 \\ \rho_s^{-1}\left(\widehat{k}_y p_{s,n} - \widehat{k}_x a\eta_{s,n}\right) & \rho_s^{-1}\left(\widehat{k}_y p_{s,T} - \widehat{k}_x a\eta_{s,T}\right) & 0 & 0 & 0 \\ \rho_s^{-1}\widehat{k}_z p_{s,n} & \rho_s^{-1}\widehat{k}_z p_{s,T} & 0 & 0 & 0 \end{pmatrix}, \tag{2.18}$$

$$D_{\alpha\beta} = \rho_s^{-1}\begin{pmatrix} 0 & 0 & 0 & 0 & 0 \\ 0 & \rho_s c_2\kappa_s & 0 & 0 & 0 \\ 0 & 0 & \sigma_s\widehat{k}_x^2 + \eta_s & \sigma_s\widehat{k}_x\widehat{k}_y & \sigma_s\widehat{k}_x\widehat{k}_z \\ 0 & 0 & \sigma_s\widehat{k}_y\widehat{k}_x & \sigma_s\widehat{k}_y^2 + \eta_s & \sigma_s\widehat{k}_y\widehat{k}_z \\ 0 & 0 & \sigma_s\widehat{k}_z\widehat{k}_x & \sigma_s\widehat{k}_z\widehat{k}_y & \sigma_s\widehat{k}_z^2 + \eta_s \end{pmatrix}, \tag{2.19}$$

where $\widehat{\mathbf{k}} = \widehat{\mathbf{k}}(t)$ is the unit vector along $\mathbf{k}(t)$, $c_1 \equiv (\gamma_s - 1)\alpha_s^{-1}$, $c_2 \equiv (mn_s C_{v,s})^{-1}$, and $\sigma_s = \frac{1}{3}\eta_s + \eta_s'$.

To simplify the analysis attention is restricted here and below to spatial perturbations only along the velocity gradient direction, i.e. $\mathbf{k} = k\,\widehat{\mathbf{y}}$. In this case the linear hydrodynamic equations have time-independent coefficients (i.e., $\mathbf{k}(t) = \mathbf{k}$),

$$\partial_t\delta\widetilde{y}_\alpha + F_{\alpha\beta}(\mathbf{k}, a)\delta\widetilde{y}_\beta = 0, \qquad F_{\alpha\beta}(\mathbf{k}, a) = \left(A(a) - ikB(a) + k^2 D\right)_{\alpha\beta}. \tag{2.20}$$

and the matrices $B(a)$ and D simplify to

$$B_{\alpha\beta}(a) = \begin{pmatrix} 0 & 0 & 0 & n_s & 0 \\ 0 & 0 & -2a\eta_s c_2 & c_1 & 0 \\ -\rho_s^{-1}a\eta_{s,n} & -\rho_s^{-1}a\eta_{s,T} & 0 & 0 & 0 \\ \rho_s^{-1}p_{s,n} & \rho_s^{-1}p_{s,T} & 0 & 0 & 0 \\ 0 & 0 & 0 & 0 & 0 \end{pmatrix}, \tag{2.21}$$

$$D_{\alpha\beta} = \begin{pmatrix} 0 & 0 & 0 & 0 & 0 \\ 0 & c_2\kappa_s & 0 & 0 & 0 \\ 0 & 0 & \rho_s^{-1}\eta_s & 0 & 0 \\ 0 & 0 & 0 & \rho_s^{-1}\left(\frac{4}{3}\eta_s + \eta_s'\right) & 0 \\ 0 & 0 & 0 & 0 & \rho_s^{-1}\eta_s \end{pmatrix}. \tag{2.22}$$

Equation (2.20) can be solved by Laplace transformation,

$$\delta\widehat{y}_\alpha(\mathbf{k}, z) = \int_0^\infty dt\, e^{-tz}\delta\widetilde{y}_\alpha(\mathbf{k}, t), \tag{2.23}$$

with the result

$$\delta\widehat{y}_\alpha(\mathbf{k}, z) = [zI + F(\mathbf{k}, a)]^{-1}_{\alpha\beta}\delta\widetilde{y}_\beta(\mathbf{k}, t = 0). \tag{2.24}$$

The eigenvalues $\omega^{(i)}(\mathbf{k}, a)$ of the matrix $F(\mathbf{k}, a)$ define the five simple hydrodynamic poles at $z = -\omega^{(i)}(\mathbf{k}, a)$. The resulting five exponentials in time represent the hydrodynamic modes for relaxation of the perturbations around uniform shear flow. At $a = 0$ (perturbations of equilibrium) they are the two sound modes, a heat mode, and a two-fold degenerate shear mode. For finite shear rate, the modes are more complicated and have qualitative differences. To illustrate, consider first the case of $k \to 0$ at fixed, finite a,

$$\omega^{(i)}(\mathbf{k}, a) \to \begin{pmatrix} b_1 k^2 \\ -\frac{1}{2}(1 + i\sqrt{3})b_2(a)k^{2/3} + \frac{1}{2}(1 - i\sqrt{3})b_3(a)k^{4/3} + b_4 k^2 \\ -\frac{1}{2}(1 - i\sqrt{3})b_2(a)k^{2/3} + \frac{1}{2}(1 + i\sqrt{3})b_3(a)k^{4/3} + b_4 k^2 \\ b_2(a)k^{2/3} + b_3(a)k^{4/3} + b_4 k^2 \\ (\eta_s/\rho_s)\, k^2 \end{pmatrix}. \tag{2.25}$$

The coefficients in these expressions are real,

$$b_1 = \left(\eta_{s,T}p_{s,n} - \eta_{s,n}p_{s,T}\right)/m\, p_{s,T}, \qquad b_2(a) = \left(2a^2\eta_s p_{s,T}/\rho_s^2 C_{v,s}\right)^{1/3},$$

$$b_3(a) = \left(2a^2\eta_s\eta_{s,T}\left(\rho_s C_{v,s}\right)^{-1} + n_s p_{s,n} + \left(\gamma_s - 1\right)\alpha_s^{-1}p_{s,T}\right)/3\rho_s\, b_2(a),$$

$$b_4 = \frac{1}{3}\left(-b_1 + \kappa_s \left(\rho_s C_{v,s}\right)^{-1} + \rho_s^{-1}\left(2\eta_s + \sigma_s\right)\right). \tag{2.26}$$

There are two diffusive modes, $\sim k^2$, but the other modes are non-analytic about $k = 0$ and represent more complex spatial dependence. This behavior can be traced to the fact that the matrix $A(a) - ikB(a)$ is not normal and cannot be diagonalized. Thus, at fixed $a \neq 0$ there is a crossover in the transformation of $F_{\alpha\beta}(\mathbf{k}, a)$ from normal diagonal form to Jordan form at small k. This is reflected in the eigenvalues if they are expanded in k at fixed a, as above. For similar reasons, care must be used in representing $\delta\widetilde{y}_\alpha(\mathbf{k}, t)$ as an expansion in the hydrodynamic modes with constant coefficients, since at small wavevectors there is a crossover to a mode expansion whose coefficients have algebraic time dependence.

The two propagating modes in (2.25) are unstable, since $b_2(a) > 0$. The above Navier-Stokes analysis applies for small but finite shear rate, and small k (long wavelength). The expansion in k verifies that the asymptotic long wavelength modes are always unstable. At larger values of k the modes are again stable, as follows from an exact evaluation of the eigenvalues. There is a critical wavevector, $k_c(a)$, such that for $k > k_c(a)$ the modes are stable whereas they are unstable otherwise. These qualitative results apply without restriction to the atomic force law, density, or temperature. Figure 1 shows $k_c(a)$ as a function of a for the special case of hard spheres at three densities, $n^* = n\sigma^3 = 0.0$, 0.2, and 0.4 (k and a measured in units of the inverse mean free path and mean free time for the hard sphere Boltzmann equation). The thermodynamic properties are calculated using the Percus-Yevick approximation, while the transport coefficients are calculated from the Enskog kinetic theory.

The instability is due to three matrix elements, B_{42}, B_{23}, and A_{34}, and is therefore present at order k. The density perturbation is constant to this order and we choose $\delta n = 0$ to simplify the discussion. The relevant variables are then the temperature perturbation δT, the longitudinal velocity perturbation δU_y, and the transverse velocity perturbation δU_x which to this order obey the equations

$$\partial_t \delta T + (\gamma_s - 1)\alpha_s^{-1}\partial_y \delta U_y - 2a\eta_s \left(\rho_s C_{v,s}\right)^{-1} \partial_y \delta U_x = 0, \tag{2.27}$$

$$\partial_t \delta U_x + a\delta U_y - \rho_s^{-1} a \eta_{s,T} \partial_y \delta T = 0, \qquad \partial_t \delta U_y + \rho_s^{-1} p_{s,T} \partial_y \delta T = 0. \tag{2.28}$$

The first equation has a coupling to the transverse velocity field due to the reference shear flow; the second equation provides a feedback to the temperature equation through the same shear flow. These couplings alone would lead simply to a renormalization of the sound velocity. However, the shear flow also couples the transverse field to the longitudinal field for an additional feedback mechanism to the temperature equation through the pressure gradient. This second mechanism is responsible for the instability. For very long wavelengths the above equations can be simplified to give

$$\partial_t^3 \delta T \sim \left(2a^2 \eta_s p_{s,T} / \rho_s^2 C_{v,s}\right) \partial_y^2 \delta T, \tag{2.29}$$

which exhibits the unstable modes of (2.25).

III. MONTE CARLO SIMULATION

The hydrodynamic description can be derived from a more fundamental level of kinetic theory. In principle, this also allows derivation of hydrodynamic equations without the restriction of the Navier-Stokes approximation to small shear rates. A model kinetic theory for the practical calculation of such generalized hydrodynamic equations is given in Ref. [10]. The resulting equations are limited to long wavelengths, as in the Navier-Stokes case, but the reference state of uniform shear flow can have a large shear rate. An analysis of the hydrodynamic modes shows that there is a critical wavevector similar to that of Figure 1. It is possible to test this hydrodynamic description by a direct simulation of the more fundamental solution to the kinetic equation. For practical reasons the simulation is more efficient at larger wavevectors and shear rates than can be justified by Navier-Stokes hydrodynamics, and this is the primary reason for considering the more complex generalized hydrodynamics.

The kinetic equation is a single relaxation time BGK equation [13] given by

$$\left(\frac{\partial}{\partial t} + \mathbf{v} \cdot \nabla_r + \nabla_v m^{-1} \cdot \mathbf{F}_{\text{ext}}\right) f(\mathbf{r}, \mathbf{v}, t) = -\nu (f(\mathbf{r}, \mathbf{v}, t) - f_\ell(\mathbf{r}, \mathbf{v}, t)). \tag{3.1}$$

Here $\mathbf{F}_{\rm ext}$ is the external force representing the thermostat, f_ℓ is the local equilibrium distribution, and ν is an average collision rate. The exact stationary solution for uniform shear flow in the presence of a thermostat has been studied in detail [14]. A variant of the Chapman-Enskog method can be used to study normal solutions for states near uniform shear flow, and to obtain the corresponding hydrodynamic equations for small perturbations relative to this state. The complete details of this solution and the hydrodynamic modes as a function of the shear rate can be found in [10]. The method of simulation is a variant of the Bird Direct Simulation method [15]. This is a Monte Carlo technique composed of two parts at each discrete time step: free streaming and collision. The volume of the system is divided into cells of dimension smaller than the mean free path, and N particles are introduced at $t = 0$ with positions and velocities sampled statistically from a specified initial distribution function. The distribution of particles is calculated at $t = \Delta t$, with Δt much smaller than the mean free time, as follows. First the particles are displaced by $\{\Delta \mathbf{r}_\mu = \mathbf{v}_\mu \Delta t\}$. Next the velocity of each particle μ is replaced with probability $\nu(n_\mu, T_\mu)\Delta t$ by a random velocity sampled from the local equilibrium distribution, $f_\ell(\{n_\mu, T_\mu, \mathbf{U}_\mu\}; \mathbf{v})$. Here n_μ, T_μ, and $\mathbf{U}_\mu$ are the density, temperature, and flow velocity in the cell containing particle μ. In this collision stage, strict conservation of momentum and energy may be violated due to statistical fluctuations. To compensate for this artificial effect, the velocities of the particles in each cell are conveniently displaced and rescaled. The whole process is then repeated for each subsequent time step. In this way, the one particle distribution function $f(\mathbf{r}, \mathbf{v}, t)$ (coarse grained over the cells) is determined, from which the hydrodynamic fields can be computed directly as averages.

In our simulations we have considered a system of size $L = 2\pi/k$, with $k = 0.1(v_0 t_0)^{-1}$, along the y-direction at a shear rate $a = 0.5 t_0^{-1}$. Here $t_0 = 1/\nu(n_s)$ is the mean free time with $\nu \propto n$ (Maxwell molecules) and $v_0 = (2k_B T_s/m)^{1/2}$ is the thermal velocity. In the remainder of this section, we take $t_0 = 1$, $v_0 = 1$, $T_s = 1$, and $n_s = 1$. Lees-Edwards boundary conditions are used to drive the shear flow [1]. These are simple periodic boundary conditions on both the position and velocity variables in the local Lagrangian frame at

$y = \pm L/2$. Both local and global thermostats have been studied. The local thermostat is the same as that of section II except that the pressure tensor is no longer limited to its Navier-Stokes form. In addition, two global thermostats are considered for more efficient implementation of the simulation. These are described in the Appendix. The analysis there and the results of the simulation show that the instability is not sensitive to the choice of thermostat. Consequently, only the results using the global thermostats are presented here. Starting from a distribution corresponding to uniform shear flow [6], the initial condition has been prepared by displacing and rescaling velocities so that

$$\delta U_{x,y}(y,0) = -\delta\widetilde{U}_{x,y}(0)\sin ky, \quad \delta U_z(y,0) = \delta n(y,0) = \delta T(y,0) = 0, \tag{3.2}$$

with $\delta\widetilde{U}_y(0) = 0.1$ and $\delta\widetilde{U}_x(0) = -0.03$. The technical parameters of the simulations are $N = 628\,000$ particles, a time step $\Delta t = 0.02$, and a cell width $\Delta L = 0.05$. The data have been averaged over 10 different realizations in the simulations of Figs. 2, 4, 6, and 7, and over 2 realizations in those of Figs. 3 and 5.

First we consider the short time dependence at a fixed position $y = -L/4$. Figure 2 shows $\delta\widetilde{U}_x(t) = \delta U_x(-L/4,t)$ and $\delta\widetilde{U}_y(t) = \delta U_y(-L/4,t)$. The dashed lines are the results from the hydrodynamic analysis of the BGK model near uniform shear flow [10]. The good agreement up to $t \approx 50$ shows that the instability is not just a consequence of the assumptions behind the hydrodynamic description. The subsequent differences between simulation and theory are due to the fact that the latter is limited to small deviations from uniform shear flow. For longer times we find both large amplitudes for δy_α and large deviations of the distribution function from that of the unperturbed state.

To investigate the asymptotic state the system, we have performed the simulations for much longer times. Figure 3 shows $\delta\widetilde{U}_x(t)$ and $\widetilde{T}(t) = T(-L/4,t)$ for time up to $t = 2000$. Both the velocity and the temperature oscillate in time and are modulated by a slowly varying amplitude relative to their asymptotic average values. The maximum value $\widetilde{T} \approx 9$ corresponds to $k \approx 0.3$, which is close to the value $k_c(a)$ at which the uniform shear flow with $a = 0.5$ would become marginally stable [9]. Thus the initial dynamics tends

toward stabilization but does not ever cross over into the stable domain. Consequently, the asymptotic dynamics is not simply that of stationary uniform shear flow at a different temperature, but rather a quasi-stationary state with different spatial structure.

The thermostat used in the above simulations allows a global change in the average temperature, which is responsible for the amplitude modulations at long times. In order to have a more controlled asymptotic state, we have considered a variation of this thermostat that maintains the average temperature constant (see the Appendix). The quantities $\delta\widetilde{U}_y(t)$ and $\widetilde{n}(t) = n(-L/4, t)$ are plotted in Fig. 4. After a transient period of length $t \approx 100$, a stable oscillatory behavior of the velocity appears with a period $\tau \simeq 54$. The shape of $\delta\widetilde{y}_\alpha$ over one cycle is shown in Fig. 5. Here $t' = t - t_{\rm tr}$, where $t_{\rm tr} = 463.4$, and the curves are averages over 20 successive cycles. The value of $t_{\rm tr}$ has been chosen as to assure that the transient time is over and also with the criterion that $\delta\widetilde{U}_x = 0$ at $t' = 0$. Inspection of the results shows several regularities. First, the following symmetry relation appears:

$$\delta\widetilde{y}_\alpha(t' + \tau/2) = \pm\delta\widetilde{y}_\alpha(t'), \tag{3.3}$$

where the minus sign applies to the velocity and the plus sign applies to the density and the temperature. Next, at times $t' \simeq 0.36\tau, 0.86\tau$, where $\delta\widetilde{U}_x$ have extrema, $\delta\widetilde{U}_y$, $\delta\widetilde{T}$, and $\delta\widetilde{n}$ seem to have nodes. Note also that the vector $\delta\widetilde{\mathbf{U}}$ rotates anti-clockwise and that most of the time $\delta\widetilde{T} > 0$ is correlated to $\delta\widetilde{n} > 0$ and $\delta\widetilde{T} < 0$ is correlated to $\delta\widetilde{n} < 0$.

The above results indicate the wave character of the asymptotic state. To confirm this point, we have analyzed the profiles of the hydrodynamic quantities at relevant times. The results are consistent with two independent invariance relations:

$$\delta y_\alpha(y, t') = \delta y_\alpha(y + L/2, t' + \tau/2), \tag{3.4}$$

$$\delta y_\alpha(y, t') = \pm\delta y_\alpha(-y, t'). \tag{3.5}$$

Their combination yields $\delta y_\alpha(y, t') = \pm\delta y_\alpha(-y - L/2, t' + \tau/2)$, which implies Eq. (3.3). Figure 6 shows the spatial variation of $\delta n(y, t')$ and $\delta T(y, t')$ at $t' =$

$0, 0.14\tau, 0.25\tau, 0.36\tau,$ and 0.5τ. Not shown are times $0.5\tau < t' < \tau$ because they can be reproduced by use of the relation (3.4). As observed in Fig. 5 for the special point $y = -L/4$ it is seen that a high (low) temperature is generally correlated to a high (low) density. The spatial distribution of the temperature is highly non-uniform even though the thermostat maintains a constant average temperature. Figure 7 shows a vector representation of the components of $\delta\mathbf{U}$ throughout the system at the values of t'. As anticipated from Fig. 5, $\delta\mathbf{U}$ rotates anti-clockwise throughout the system. The layers $y = 0, \pm L/2$ are always nodes of $\delta\mathbf{U}$ and extrema of δT and δn. The pattern indicated by Figs. 6 and 7 can be described as a periodic standing wave represented by the superposition of two symmetrical waves travelling in opposite directions.

In summary, for initial values of k and a in the predicted unstable domain small perturbations of the hydrodynamic fields grow according to the linear hydrodynamic equations for $t < 50$. Subsequently, non-linear effects invalidate this theoretical analysis. The simulations show a transient period up to about $t \approx 100$, after which a quasi-stationary state is observed for $100 < t \leq 2000$. In this asymptotic state the vector quantities oscillate at a period approximately twice that of the scalar fields. The oscillations are spatially non-uniform for all fields considered.

IV. MOLECULAR DYNAMICS SIMULATION

The most extensive prior studies of uniform shear flow have been for dense systems via molecular dynamics (MD) simulations. No signature of the instability discussed here has been noted in these previous results. There are two significant differences between the theory and simulation discussed above and the detailed implementation of earlier MD simulations. The first, and perhaps most important, has been the consideration of small system sizes relative to the wavelengths necessary to see the instability. Typically, system size is determined by the simulation time such that a sound wave will not traverse the system and generate correlations. At high densities this has led to consideration of system

sizes small compared to the critical wavevector for instability. A second difference from the discussion above is the method for imposing a thermostat. In MD simulations it is efficient to impose the temperature control by a global re-scaling of the velocities only after as many as 100 collisions. However, at the shear rates considered this implies significant heating between applications of the thermstat and the temperature is more like a sawtooth in time rather than constant. Thus it is difficult to give a direct theoretical correspondence to the MD simulation results.

To demonstrate the existence of the instability using MD simulations we have considered a rectangular unit cell with one side expanded 15 times larger than the other two (1620 hard spheres of diameter σ at a density of $n\sigma^3 = 0.5$ in a cell of size $6\sigma \times 90\sigma \times 6\sigma$). The Lees-Edwards boundary conditions are applied on the x, z surfaces so that the velocity gradient is along the larger dimension of the system, allowing study of much longer wavelengths in the direction of the gradient than have previously been considered. A second difference from previous simulations is a more frequent application of the velocity scaling to control the themperature and better represent continuous cooling. In our simulations the velocities are rescaled whenever the temperature differs by 5% from its set value. The simulation cell is divided into a fixed number of subcells, the local velocity field in each subcell is calculated and the excess kinetic energy computed relative to the local velocity field. The velocities of the particles in each subcell are then rescaled so that the total excess kinetic energy of each subcell is equal to the set value. The amount of rescaling is determined locally, and thus corresponds to a local thermostat, $\lambda(\mathbf{r}, t) = \lambda[n(\mathbf{r}, t), T(\mathbf{r}, t)]$, as discussed in the Appendix. Our implementation follows Hess [4] in that we assume uniformity of all quantities in the directions perpendicular to the velocity gradient so that the subcells are thin slabs and the only spatial variations are in the direction of the velocity gradient, as in the Monte Carlo simulations. Due to the large number of particles in the simulations, the length of the simulations is relatively modest $t \approx 5 \times 10^5$ collisions. The shear rate was fixed at $a = 1.77\sqrt{k_B T/m\sigma^2}$ and an initial perturbation with $k_y = 2\pi/L_y$ was monitored. Our theoretical estimates indicate this should correspond to conditions of instability. Figure

8 shows the x-component of the velocity field growing steadily throughout the simulation, clearly indicating the instability. Conversely, perturbations with a wavelength one quarter of this value appear to be stable as expected. Similar results are observed for the density field as well. Our primary conclusion from these preliminary results is that the instability can be observed and studied by MD simulations if larger system sizes are considered and more care is taken with application of the thermostat.

V. DISCUSSION

Uniform shear flow has been a prototype state for the study of fluids far from equilibrium, using both theoretical and computer simulation methods. Until recently, it has been assumed that this state is stable except at high densities and short wavelengths. The new results reported here and in [9,10] show that this simple macroscopic state is unstable at sufficiently large wavelengths. Previous studies via simulation have not seen this instability due to finite system sizes. However, theoretical analysis at the hydrodynamic level clearly shows the mechanism and parameter space for this instability. In the present work this theoretical analysis is tested both qualitatively and quantitatively. At the qualitative level, both Monte Carlo simulations of a kinetic theory description and molecular dynamics simulation of the Newtonian dynamics show clearly that this flow is unstable at long wavelengths. The Monte Carlo simulation also confirms quantitatively the predictions of the theory on the time scale for which the linear analysis is valid. At longer times the Monte Carlo simulation shows clearly that the asymptotic state is spatially non-uniform with a periodic variation in time. A precise theoretical description of this final state has not been developed at this time.

The analysis here has been limited to spatial perturbations along the gradient of the velocity in the stationary state. More general perturbations will lead to more complex flows due to the coupling to the convective flow. A theoretical analysis of this more general case is in progress but is significantly more complex. Due to the fact that the $k = 0$ matrix of the hydrodynamic equations is non-diagonalizable (non-normal), the corresponding eigenvalues

do not fix a unique eigenspace. The resulting dynamics is not simply a superposition of decaying or growing modes, but rather includes as well algebraic growth. The resulting analysis of conditions for instability is more complex and will be reported elsewhere.

ACKNOWLEDGMENTS

The research of M.L. and J.D. was supported in part by NSF grant PHY 9312723. The research of J.M.M. and A.S. was supported in part by the DGICYT (Spain) and by the Junta de Extremadura-Fondo Social Europeo through Grants No. PB94-1021 and No. EIA94-39, respectively. Partial support for this research also was provided by the Division of Sponsored Research at the University of Florida.

APPENDIX: ROLE OF THE THERMOSTAT

The analysis of section II made use of a specific choice for the thermostat. Other choices are possible and more convenient for computer simulation. In this work we use two different types of thermostats, both obtained from an external force at the microscopic level of the form

$$\mathbf{F}_{\rm ext}(\mathbf{r},t) = -m\lambda(n(\mathbf{r},t),T(\mathbf{r},t))[\mathbf{v}-\mathbf{U}(\mathbf{r},t)]. \tag{A1}$$

The corresponding source term w in the temperature equation (2.2) is

$$w(n(\mathbf{r},t),T(\mathbf{r},t)) = -2K(n(\mathbf{r},t),T(\mathbf{r},t))\lambda(n(\mathbf{r},t),T(\mathbf{r},t)), \tag{A2}$$

where $K(n(\mathbf{r},t),T(\mathbf{r},t))$ is the kinetic energy density. The thermostat parameter, $\lambda(n(\mathbf{r},t),T(\mathbf{r},t))$, is always chosen to ensure constant temperature in the reference state, $\lambda_s = \lambda(n_s,T_s) = -aP_{s,xy}/2K_s$, as follows from (2.5). In this work we use three different thermostats, one local and two global. The local thermostat is defined by $\lambda(n(\mathbf{r},t),T(\mathbf{r},t)) \to \lambda_s + \lambda_{s,n}\delta n(\mathbf{r},t) + \lambda_{s,T}\delta T(\mathbf{r},t)$, to linear order, so that

$$w_1(n(\mathbf{r},t),T(\mathbf{r},t)) \to -2K_s\lambda_s - 2\left(K\lambda\right)_{s,n}\delta n(\mathbf{r},t) - 2\left(K\lambda\right)_{s,T}\delta T(\mathbf{r},t). \tag{A3}$$

The coefficients $\lambda_{s,n}$ and $\lambda_{s,T}$ are chosen such that all viscous heating proportional to $\delta n(\mathbf{r},t)$ and $\delta T(\mathbf{r},t)$ is compensated by the source term. While there is still a local temperature variation, this thermostat holds the average temperature constant. It is this local thermostat that is used in section II, with P_{xy} approximated by its Navier-Stokes form. The other two thermostats considered are global, i.e. the parameter λ is spatially constant. The simplest case is $\lambda = \lambda_s$ with a corresponding source term

$$w_2(n(\mathbf{r},t),T(\mathbf{r},t)) \to -2K_s\lambda_s - 2\lambda_s K_{s,n}\delta n(\mathbf{r},t) - 2\lambda_s K_{s,T}\delta T(\mathbf{r},t). \tag{A4}$$

In this case there are greater effects due to viscous heating by the perturbations than with the choice w_1, and even the average temperature of the system changes except at the stationary state. A second global thermostat eliminates this global change using the form, $\lambda \to \lambda_s + \lambda_{s,n}\delta\overline{n} + \lambda_{s,T}\delta\overline{T}$, where $\delta\overline{n}$ and $\delta\overline{T}$ are the volume averaged density and temperature. The source term in this case is

$$w_3(n(\mathbf{r},t),T(\mathbf{r},t)) \to w_2(n(\mathbf{r},t),T(\mathbf{r},t)) - 2K_s\left[\lambda_{s,n}\delta\overline{n} + \lambda_{s,T}\delta\overline{T}\right]. \tag{A5}$$

In Fourier representation the sources w_2 and w_3 are the same except for the $k = 0$ dynamics.

Both theory and the Monte Carlo simulations of section III indicate that the details of the perturbed dynamics depend on the thermostat used, but that the mechanisim for the instability is insensitive to the choice of thermostat. To illustrate this we repeat the analysis of section II using the global thermostat (A4) (again in the Navier-Stokes limit). There are two new terms in the temperature equation. One is due to temperature perturbations and leads to viscous heating even for uniform perturbations. The second is due to density perturbations and provides a direct k - independent coupling of the temperature and density equations (at zero shear rate the density and temperature are only coupled indirectly via the gradients of the longitudinal velocity component and the pressure). The matrices $B(a)$ and D are unchanged from section II, but these new couplings replace A_{21} and A_{22} in (2.17) with non-zero values proportional to a^2,

$$\begin{pmatrix} A_{21}(a) \\ A_{22}(a) \end{pmatrix} \rightarrow \begin{pmatrix} -c_2\left(a^2\eta_{s,n} + w_n\right) \\ -c_2\left(a^2\eta_{s,T} + w_T\right) \end{pmatrix}, \tag{A6}$$

where $w_n \equiv \partial w(n_s, T_s)/\partial n_s$, $w_T \equiv \partial w(n_s, T_s)/\partial T_s$. The matrix $A(a) - ikB(a)$ is now diagonalizable and an expansion of the hydrodynamic modes in powers of k rather than $k^{2/3}$ is obtained,

$$\omega^{(i)}(\mathbf{k}, a) \rightarrow \begin{pmatrix} A_{22}(a) + d_1(a)k^2 \\ d_2(a)k^2 \\ ic(a)k - \left(d_3(a)/a^2 - d_4(a)\right)k^2 \\ -ic(a)k - \left(d_3(a)/a^2 - d_4(a)\right)k^2 \\ \left(\eta_s/\rho_s\right)k^2 \end{pmatrix}, \tag{A7}$$

with the coefficients,

$$d_1(a) = \kappa_s c_2 + \frac{2a^2 c_2 \eta_s \eta_{s,T} + c_1 p_{s,T}}{\rho_s c_2(\eta_{s,T}a^2 + w_T)} + \frac{p_{s,T}(n_s\eta_{s,n}a^2 + n_s w_n + 2\eta_s a^2)}{\rho_s c_2(\eta_{s,T}a^2 + w_T)^2},$$

$$d_2(a) = -\frac{\eta_s\left[p_{s,n}\left(a^2\eta_{s,T} - w_T\right) + p_{s,T}\left(-a^2\eta_{s,n} + w_n\right)\right]}{m\left[n_s p_{s,n}\left(a^2\eta_{s,T} + w_T\right) - p_{s,T}\left(a^2 n_s\eta_{s,n} + n_s w_n + 2\eta_s a^2\right)\right]},$$

$$c^2(a) = \frac{\left[n_s p_{s,n}\left(a^2\eta_{s,T} + w_T\right) - p_{s,T}\left(a^2 n_s\eta_{s,n} + n_s w_n + 2\eta_s a^2\right)\right]}{\rho_s\left(a^2\eta_{s,T} + w_T\right)},$$

$$d_3(a) = \frac{p_{s,T}a^2}{2\rho_s c_2\left(a^2\eta_{s,T} + w_T\right)}\left[c_1 + \frac{\left(a^2 n_s\eta_{s,n} + n_s w_n + 2\eta_s a^2\right)}{\left(a^2\eta_{s,T} + w_T\right)}\right],$$

$$d_4(a) = -\frac{1}{2}\,d_2(a) - \frac{a^2\eta_s\eta_{s,T}}{\rho_s\left(a^2\eta_{s,T} + w_T\right)} + \frac{2\eta_s + \sigma_s}{2\rho_s}. \tag{A8}$$

There are two diffusive modes, two propagating sound modes, and a time-modulated diffusive mode. The sound modes are unstable at long wavelengths for shear rates satisfying $d_3(a) - a^2 d_4(a) > 0$. This possibility has been explored in reference [9] for the special case of hard spheres. In that case both $d_3(a)$ and $d_4(a)$ are positive and the modes are unstable for sufficiently small shear rates. The corresponding critical wavevector, $k_c(a)$, for

this thermostat is determined from the exact eigenvalues and shown in Figure 9 for the same densities as in Figure 1. The domain of instability at long wavelengths is similar to that of Figure 1 using the thermostat w_1.

The thermostat of this Appendix allows greater viscous heating than that of section II for states perturbed from uniform shear flow. The hydrodynamic modes are quite different, reflecting a sensitivity to the choice of thermostat. These qualitative differences can be traced to the mathematical differences between diagonalizable and non-diagonalizable matrices, $A_{\alpha\beta}$. Nevertheless, the mechanism for the instability described at the end of section II remains effective in both cases. These conclusions are not limited to the Navier-Stokes approximation, but are confirmed as well for the kinetic model results described in section III for larger shear rates.

REFERENCES

[1] A. W. Lees and S. F. Edwards, J. Phys. C **5**, 1921 (1972).

[2] J. W. Dufty, J. J. Brey, and A. Santos in *Molecular Dynamics Simulation of Statistical Mechanical Systems*, edited by G. Ciccotti and W. G. Hoover (North Holland Publ. Co., Amsterdam, 1986), pp. 295–303.

[3] J. W. Dufty, A. Santos, J. J. Brey, and R. F. Rodríguez, Phys. Rev. A **33**, 459 (1986).

[4] For extensive references see D. J. Evans and W. Hoover, Ann. Rev. Fluid Mech. **18**, 243 (1986); W. Loose and S. Hess in *Microscopic Simulation of Complex Flows*, M. Mareschal ed. (Plenum Press, New York, 1990), pp. 267-278.

[5] J. G. Ordóñez, J. J. Brey, and A. Santos, Phys. Rev. A **41**, 810 (1990).

[6] J. M. Montanero, A. Santos, and V. Garzó, Phys. Fluids **8**, 1981 (1996).

[7] J. Erpenbeck, Phys. Rev. Lett. **52**, 1333 (1984).

[8] J. F. Lutsko and J. W. Dufty, Phys. Rev. Lett. **57**, 2775 (1986); J. F. Lutsko, J. W. Dufty, and S. P. Das, Phys. Rev. A **39**, 1311 (1989); T. Kirkpatrick and J. C. Nieuwoudt, Phys. Rev. Lett. **56**,885 (1986).

[9] M. Lee, J. W. Dufty, J. M. Montanero, A. Santos, and J. F. Lutsko, Phys. Rev. Lett. **76**, 2702 (1996).

[10] M. Lee and J. W. Dufty, Phys. Rev. E (to be published).

[11] J. W. Dufty, A. Santos, and J. J. Brey, Phys. Rev. Lett. 77, 1270 (1996); J. W. Dufty, J. J. Brey, and A. Santos, Physica (in press); J. F. Lutsko, Phys. Rev. Lett. **78**, 243 (1997).

[12] J.A. McLennan, *Introduction to Non-equilibrium Statistical Mechanics* (Prentice Hall, Englewood Cliffs, NJ, 1989).

[13] C. Cercignani, *Mathematical Methods in Kinetic Theory* (Plenum Press, New York, 1990).

[14] A. Santos and J. J. Brey, Physica A **174**, 355 (1991).

[15] G. A. Bird, *Molecular Gas Dynamics and the Direct Simulation of Dense Flows* (Clarendon Press, Oxford, 1994).

FIGURES

FIG. 1. Critical lines for stability for hard spheres at $n^* = 0.0$ (solid curve), $n^* = 0.2$ (dashed curve), and $n^* = 0.4$ (dashed-dotted curve) with the local thermostat.

FIG. 2. Plot of $\delta\widetilde{U}_x(t)$ and $\delta\widetilde{U}_y(t)$. The solid lines are simulation results and the dashed lines correspond to the analysis of Ref. [10].

FIG. 3. Plot of $\delta\widetilde{U}_x(t)$ and $\delta\widetilde{T}(t)$.

FIG. 4. Plot of $\delta\widetilde{U}_y(t)$ and $\delta\widetilde{n}(t)$.

FIG. 5. Plot of $\delta\widetilde{y}_\alpha(t')$ over one cycle.

FIG. 6. $T(y,t')$ and $n(y,t')$ as a function of y for (from top to bottom) $t' = 0, 0.14\tau, 0.25\tau, 0.36\tau,$ and 0.5τ.

FIG. 7. Vector plot representing $\delta U_x(y,t')$ and $\delta U_y(y,t')$ at $t' = 0, 0.14\tau, 0.25\tau, 0.36\tau,$ and 0.5τ.

FIG. 8. The long-wavelength component of the velocity in the flow direction as a function of time from molecular dynamics simulation. Units are $m = \sigma = k_B T = 1$.

FIG. 9. Critical lines for stability for hard spheres for the same densities as in Fig. 1 with the global thermostat (A4).

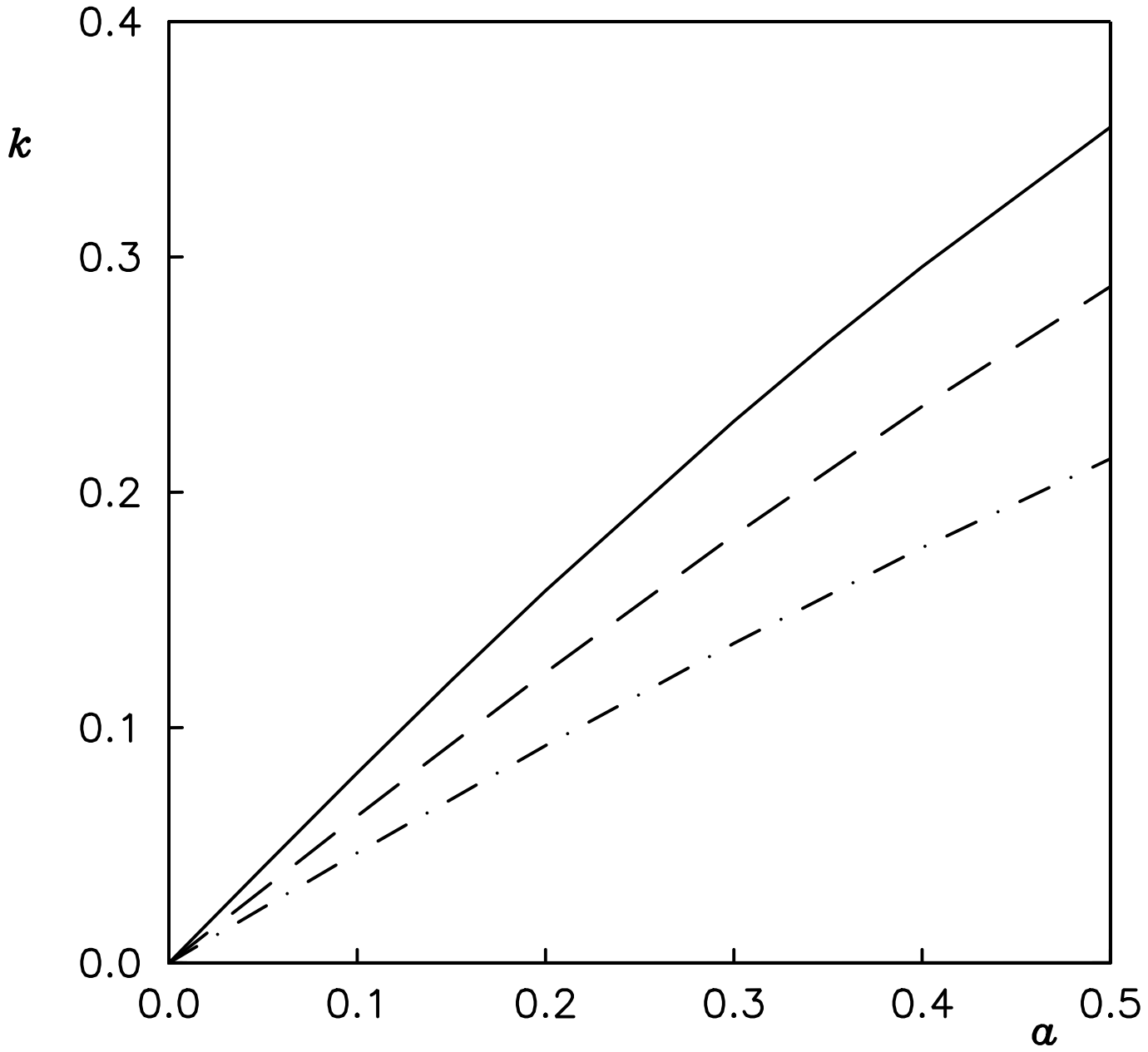
0.4
k
0.3
0.2
0.1
0.0
0.0
0.1
0.2
0.3
0.4
0.5
a

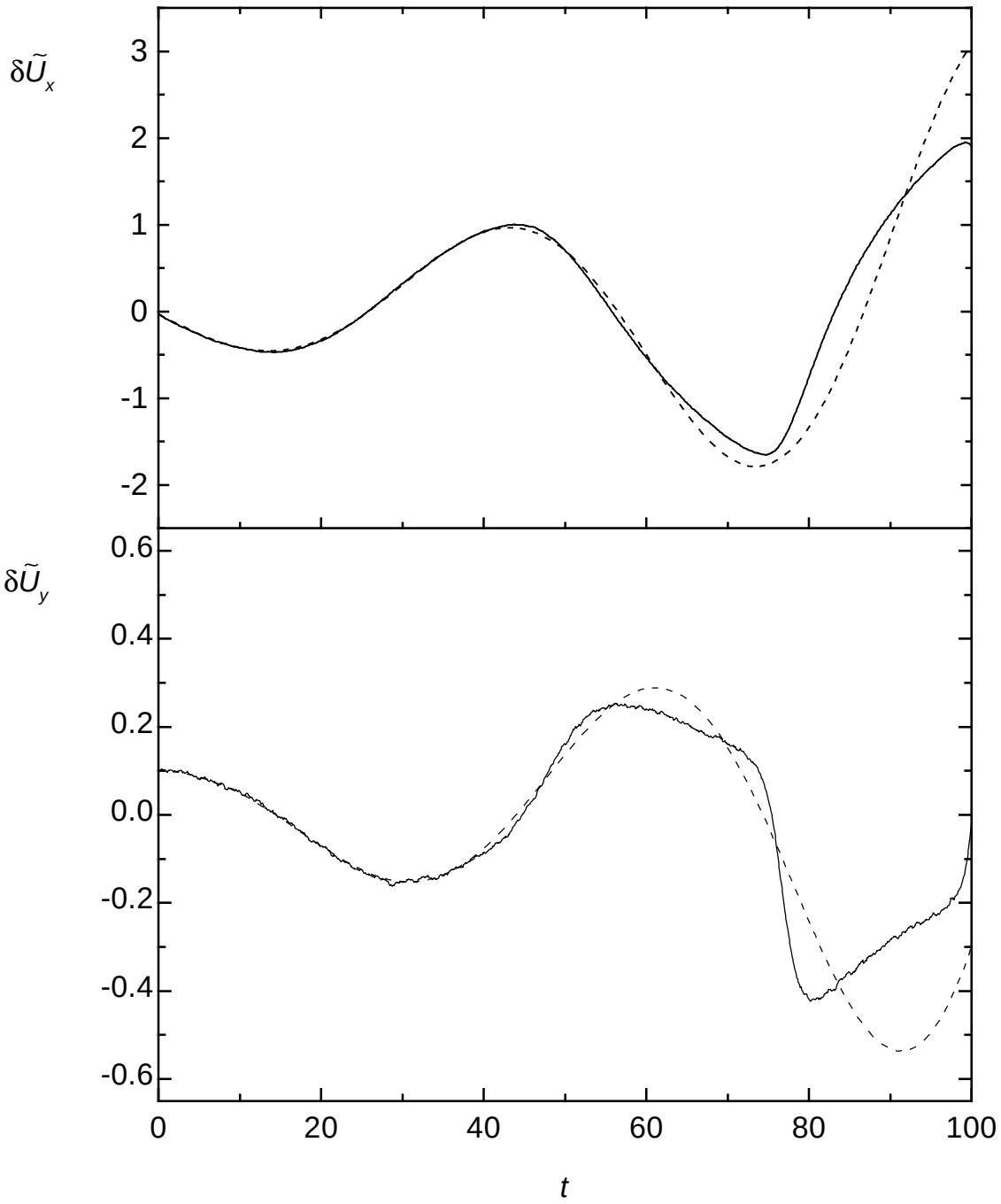
$\delta\widetilde{U}_x$
3
2
1
0
-1
-2
$\delta\widetilde{U}_y$
0.6
0.4
0.2
0.0
-0.2
-0.4
-0.6
0
20
40
60
80
100
t

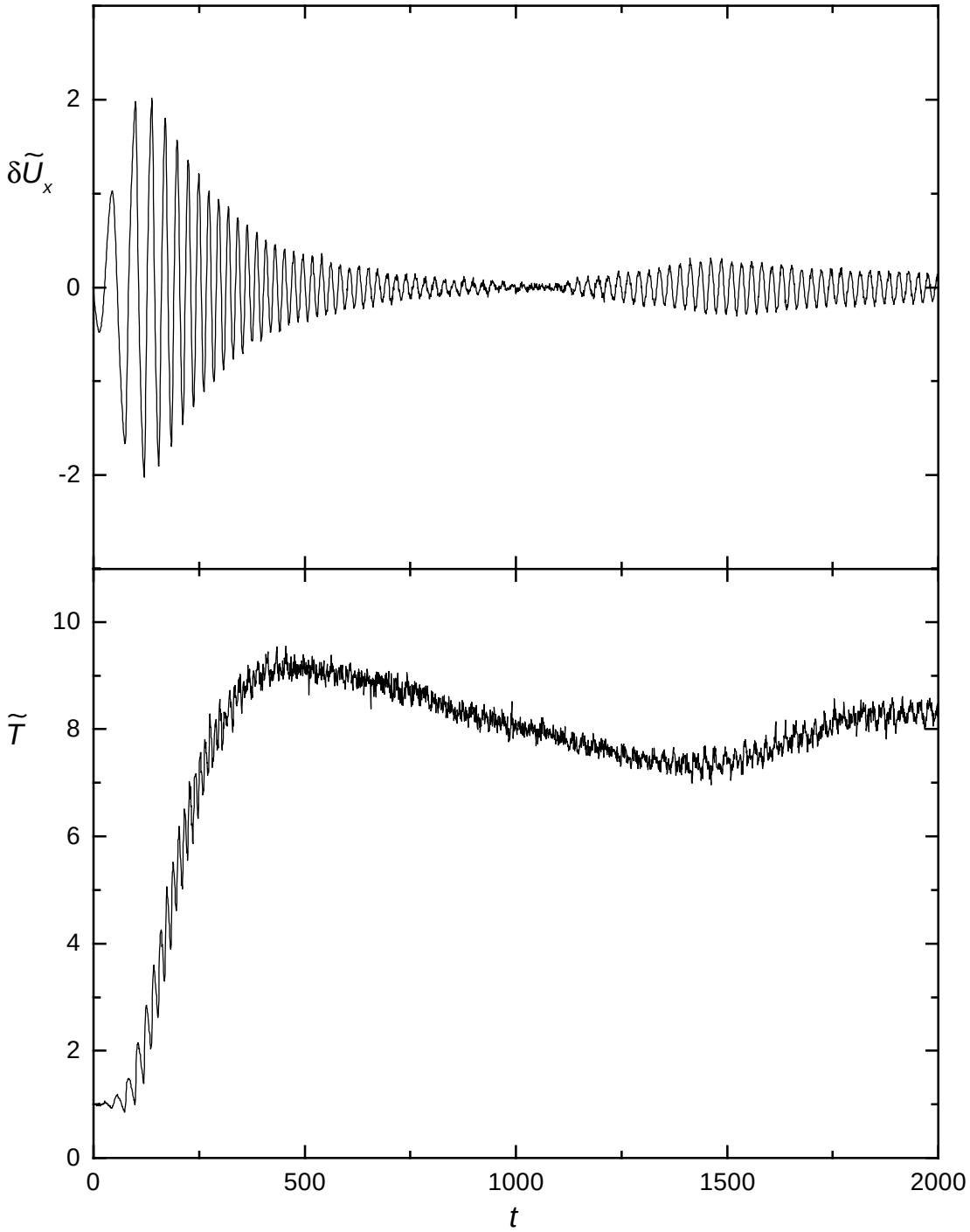
$\delta\widetilde{U}_x$
2
0
-2
$\widetilde{T}$
10
8
6
4
2
0
0
500
1000
1500
2000
t

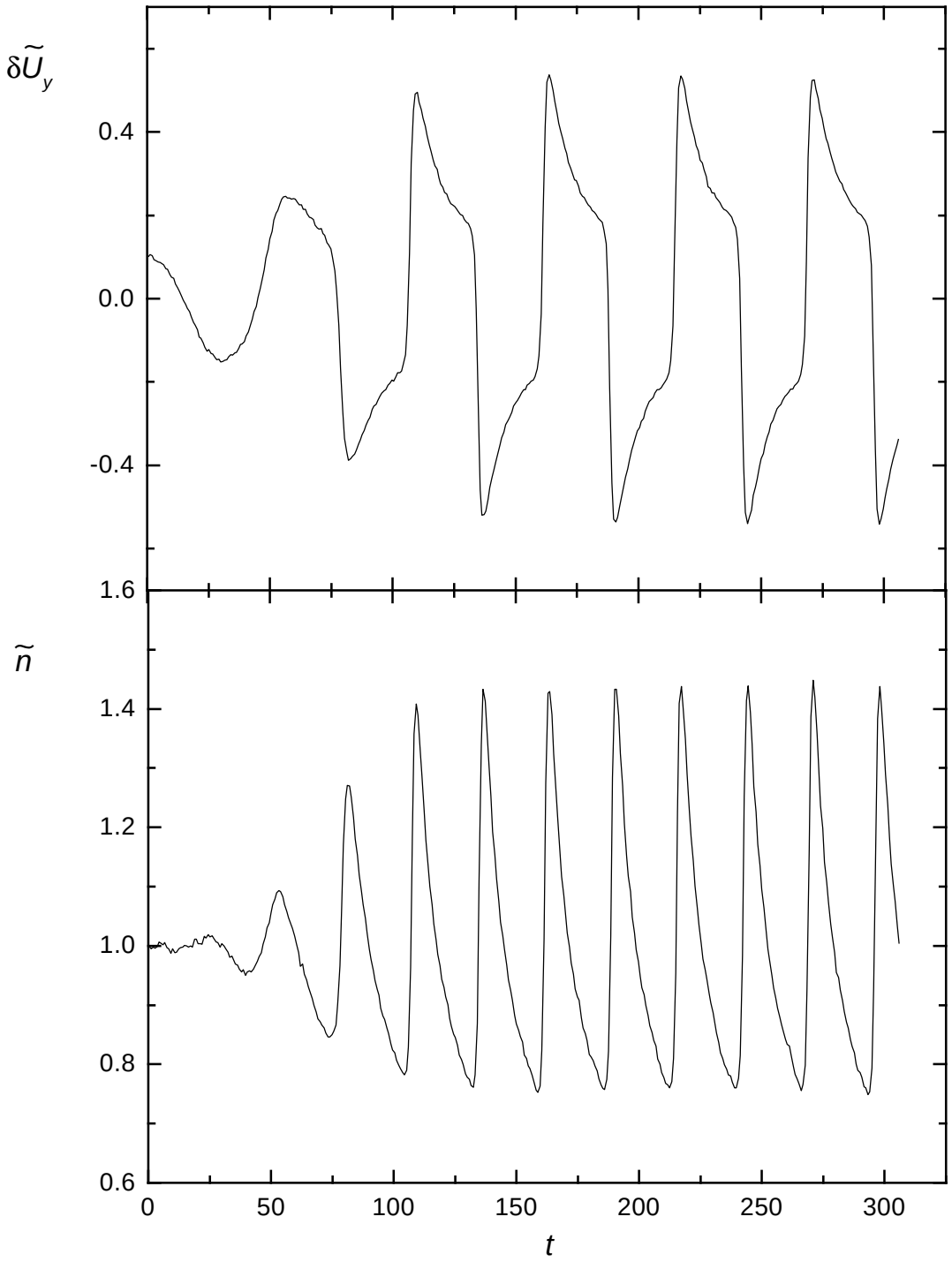
$\delta\widetilde{U}_y$
0.4
0.0
-0.4
1.6
$\widetilde{n}$
1.4
1.2
1.0
0.8
0.6
0
50
100
150
200
250
300
t

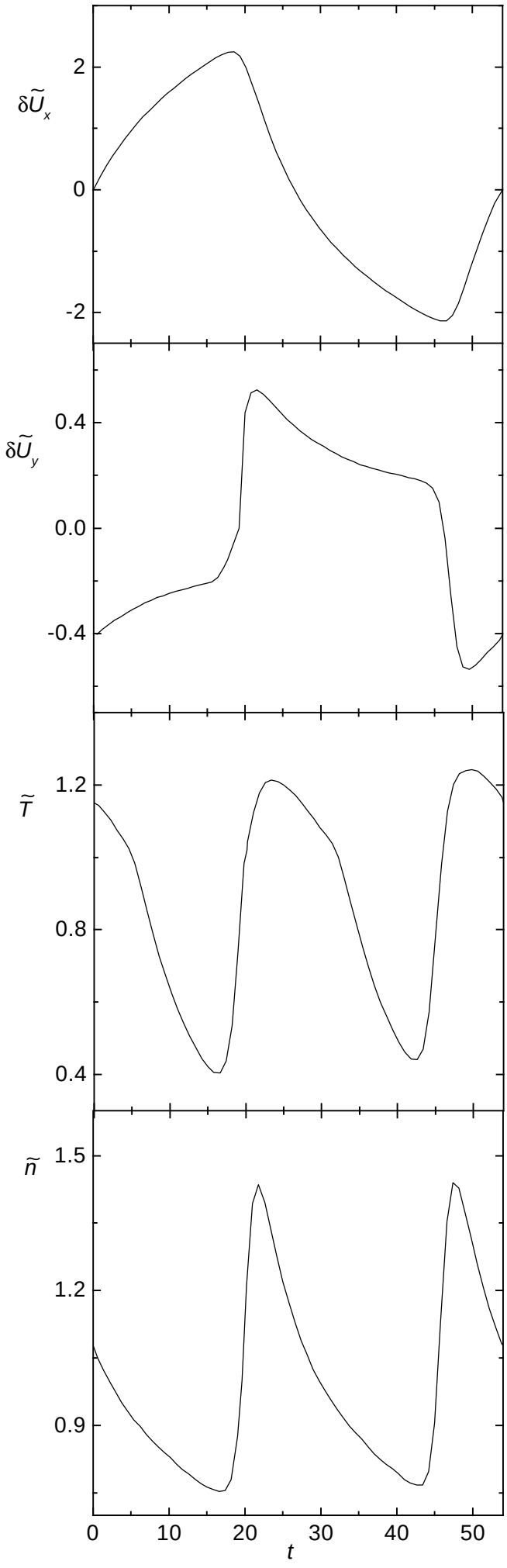
$\delta\widetilde{U}_x$
2
0
-2
$\delta\widetilde{U}_y$
0.4
0.0
-0.4
$\widetilde{T}$
1.2
0.8
0.4
$\widetilde{n}$
1.5
1.2
0.9
0
10
20
30
40
50
t

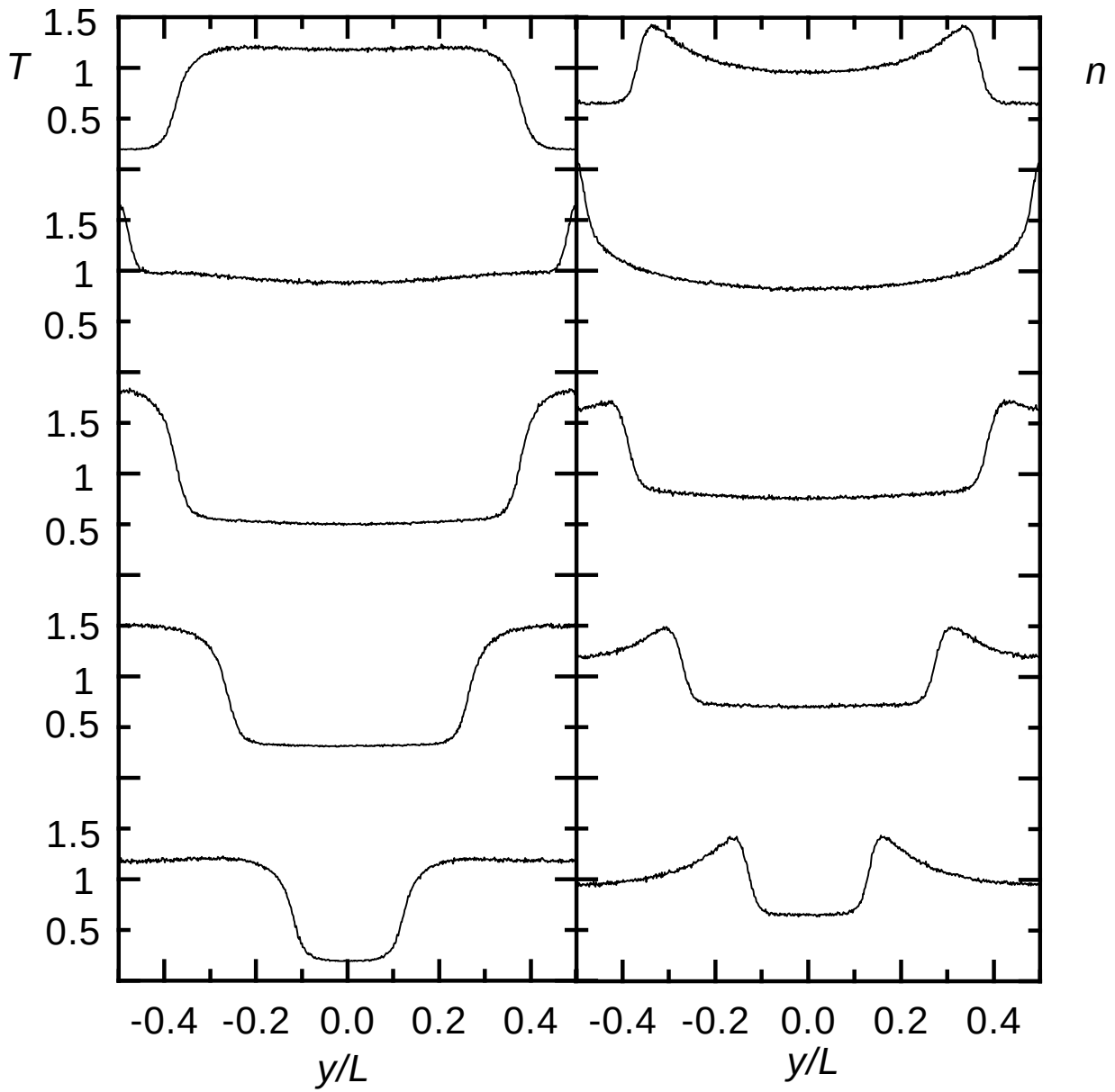
T
n
1.5
1
0.5
-0.4
-0.2
0.0
0.2
0.4
y/L

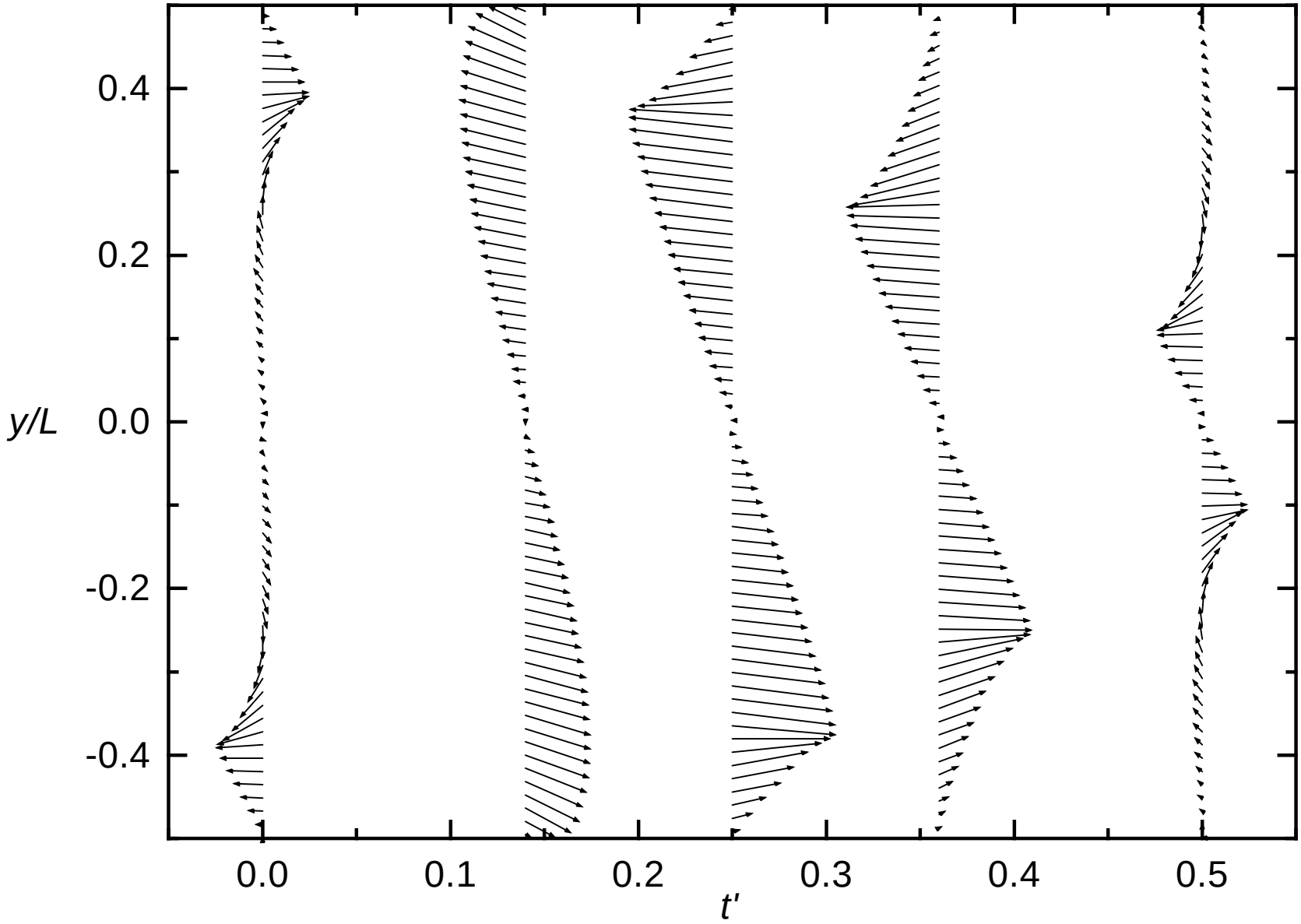
0.4
0.2
0.0
-0.2
-0.4
y/L
0.0
0.1
0.2
0.3
0.4
0.5
t'

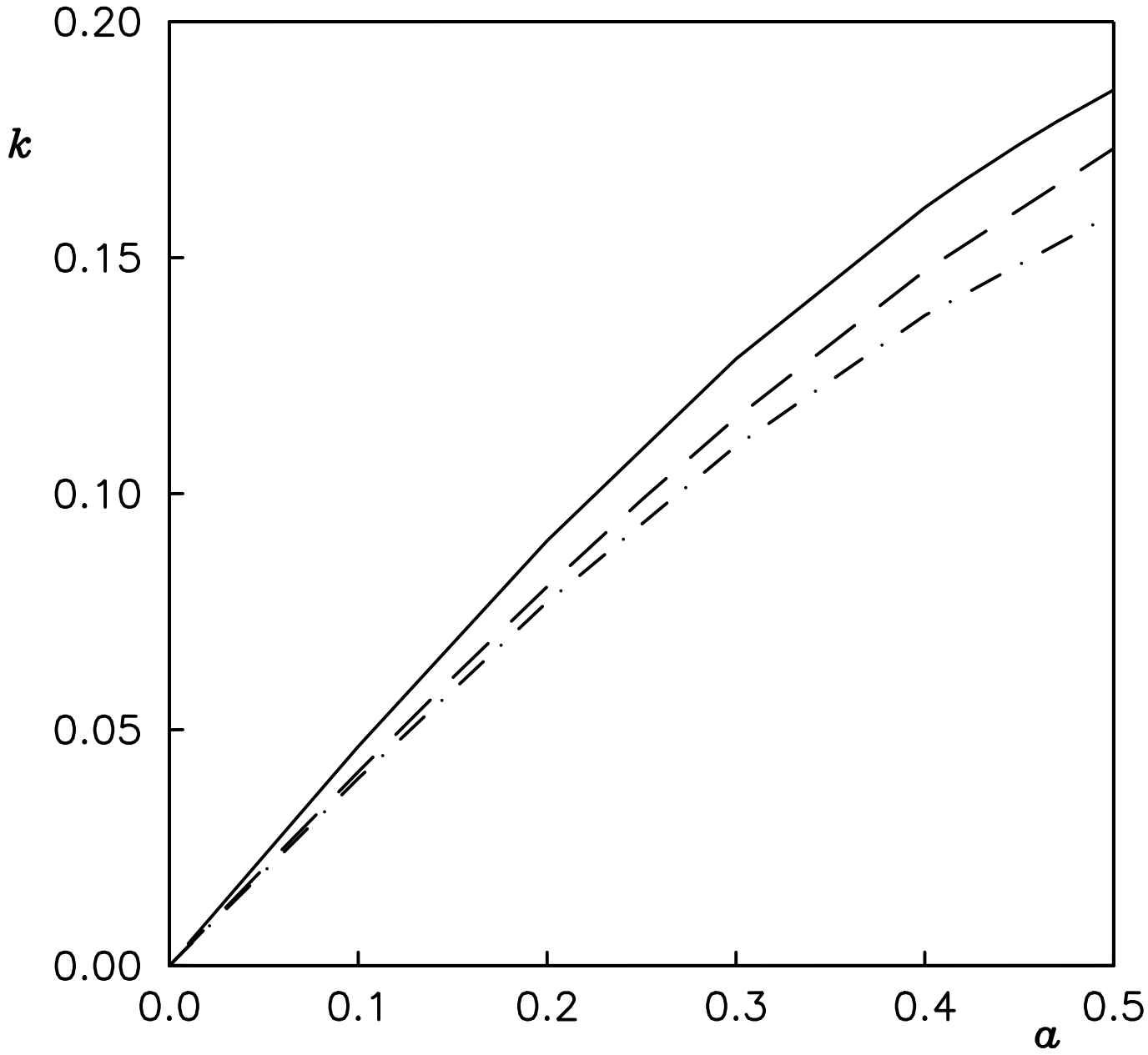
0.20
k
0.15
0.10
0.05
0.00
0.0
0.1
0.2
0.3
0.4
0.5
a